Short communication

Nano-Sn/hard carbon composite anode material with high-initial coulombic efficiency

Bingkun Guo, Jie Shu, Kun Tang, Ying Bai, Zhaoxiang Wang*, Liquan Chen

Laboratory for Solid State Ionics, Institute of Physics, Chinese Academy of Sciences, Beijing 100080, China

Abstract

Nanoscaled tin (Sn) particles were embedded in the mesopores of hard carbon spherules (HCS) to form a composite anode material for lithium ion batteries. The structure of the obtained composite was characterized by X-ray diffraction (XRD) and the electrochemical performances were evaluated by galvanostatic cycling and cyclic voltammetry. It is found that embedding Sn nanoparticles into HCS not only results in a composite material with high-lithium storage capacity and capacity retention, but also increases the initial coulombic efficiency of the composite. Based on the infrared spectroscopic analysis, the enhanced initial coulombic efficiency is attributed to the nano-tin-induced decomposition of the $ROCO_2Li$ species in the solid electrolyte interphase (SEI) layer.
© 2007 Elsevier B.V. All rights reserved.

Keywords: Hard carbon spherule; Composite; Lithium ion battery; High-initial coulombic efficiency

1. Introduction

Low-temperature pyrolytic hard carbons are promising anode materials for lithium ion batteries. The disordered structures guarantee their high-structural stability during repeated cycling while their nanopores provide possible active sites for hosting hetero nanoparticles [1]. However, the initial coulombic efficiency of the hard carbon anodes is usually low (∼60%) due to the formation of a thick solid electrolyte interphase (SEI) layer, which consumes lots of the lithium ions supplied by the cathode material [2,3]. As the formation of an SEI layer is unavoidable, refeeding the lithium ions back to the cathode from the SEI layer becomes an important way to increase the initial coulombic efficiency and therefore, the specific capacity, of the battery.

Nanosized tin (Sn) is also a well-known promising anode material with very high-lithium storage capacities by forming $Li_{4.4}Sn$ alloy [4]. However, similar to other nanoscaled particles, it suffers severe aggregation during cycling, leading to quick capacity decay. By pinning the nanoparticles on the surface or embedding them in the mesopores of the hard carbon, the aggregation can be effectively suppressed [5,6]. In our previous work, a composite anode material with high capacity and capacity retention was prepared by embedding nano-Co_3O_4 particles in the mesopores on the surface of hard carbon spherules (HCS) [7]. However, the mesopores are only distributed on the surface of the HCS. Therefore, the initial coulombic efficiency of the composite and the content of the embedded Co_3O_4 remain low.

In this work, iron was used to expand the nanopores in the HCS to mesopores by catalyzing the reaction between H_2O vapor and C [8]. Sn nanoparticles were embedded in these mesopores to form a homogeneous HCS/Sn composite.

2. Experimental

Sugar was used as the precursor of the HCS. Details for the preparation of the HCS with a diameter of 5–10 μm have been described elsewhere [9]. $Fe(NO_3)_3$ was added into the sugar precursor and reduced to Fe during low-temperature pyrolysis. With the catalysis effect of Fe, the HCS was activated with H_2O vapor at 900 °C for 2 h and its nanopores were expanded to mesopores. Then, the porous HCS was added into the solution of $SnCl_4$ dissolved in ethanol. The mixture was hydrothermally processed in a stainless steel autoclave at 140 °C for 5 h. The obtained black powder was reduced in a tube furnace in an Ar/H_2 atmosphere at 900 °C for 3 h. Considering that the embedded

* Corresponding author. Tel.: +86 10 82649050; fax: +86 10 82649050.
 E-mail address: zxwang@aphy.iphy.ac.cn (Z. Wang).

tin nanoparticles are sensitive to oxygen, a layer of soft-carbon was coated on the HCS/Sn composite (HCS–Sn–C) by further heating these HCS particles at 800 °C for 2 h in acetylene.

The structure of the obtained HCS–Sn–C composite was characterized by X'Pert Pro MPD X-ray diffractometer equipped with a monochromatized Cu Kα1 radiation source ($\lambda = 1.5418$ Å) and the morphology was observed on a Hitachi S-4000 scanning electron microscope (SEM). Each Fourier transformed infrared (FTIR) spectrum was the average of 400 scans on a BIO-RAD FTS-60 spectrometer.

Test cells were assembled in an Ar-filled glove box (MBraun, Lab Master 130) for evaluating the electrochemical performances of the composite. The working electrode was prepared by casting a mixture of the HCS–Sn–C (90 wt.%), polyvinylidene fluoride (PVDF, 5 wt.%) dissolved in *N*-methylpyrrolidone (NMP) and carbon black (5 wt.%) on a copper foil. The foil was

then dried under vacuum at 100 °C for 8 h. Li foil was used as the counter electrode, 1 mol L^{-1} LiPF$_6$ dissolved in a mixture of ethylene carbonate (EC) and dimethyl carbonate (DMC) (1:1 in volume) as the electrolyte, and Celgard 2400 as the separator. The cell was galvanostatically cycled between 0.0 and 2.5 or 3.0 V (*vs.* Li) at a current density of 0.1 mA cm^{-2}. Cyclic voltammetry (CV) was carried out on a CH Instruments electrochemical workstation (Model 660A) at a scanning rate of 0.05 mV s^{-1}.

3. Results and discussion

Fig. 1a shows the morphology of the HCS. The bright dots are iron particles uniformly distributed on the HCS surface. By dissection with the focused ion beam (FIB) technique, the iron nanoparticles within the HCS particle are also *in situ* observed
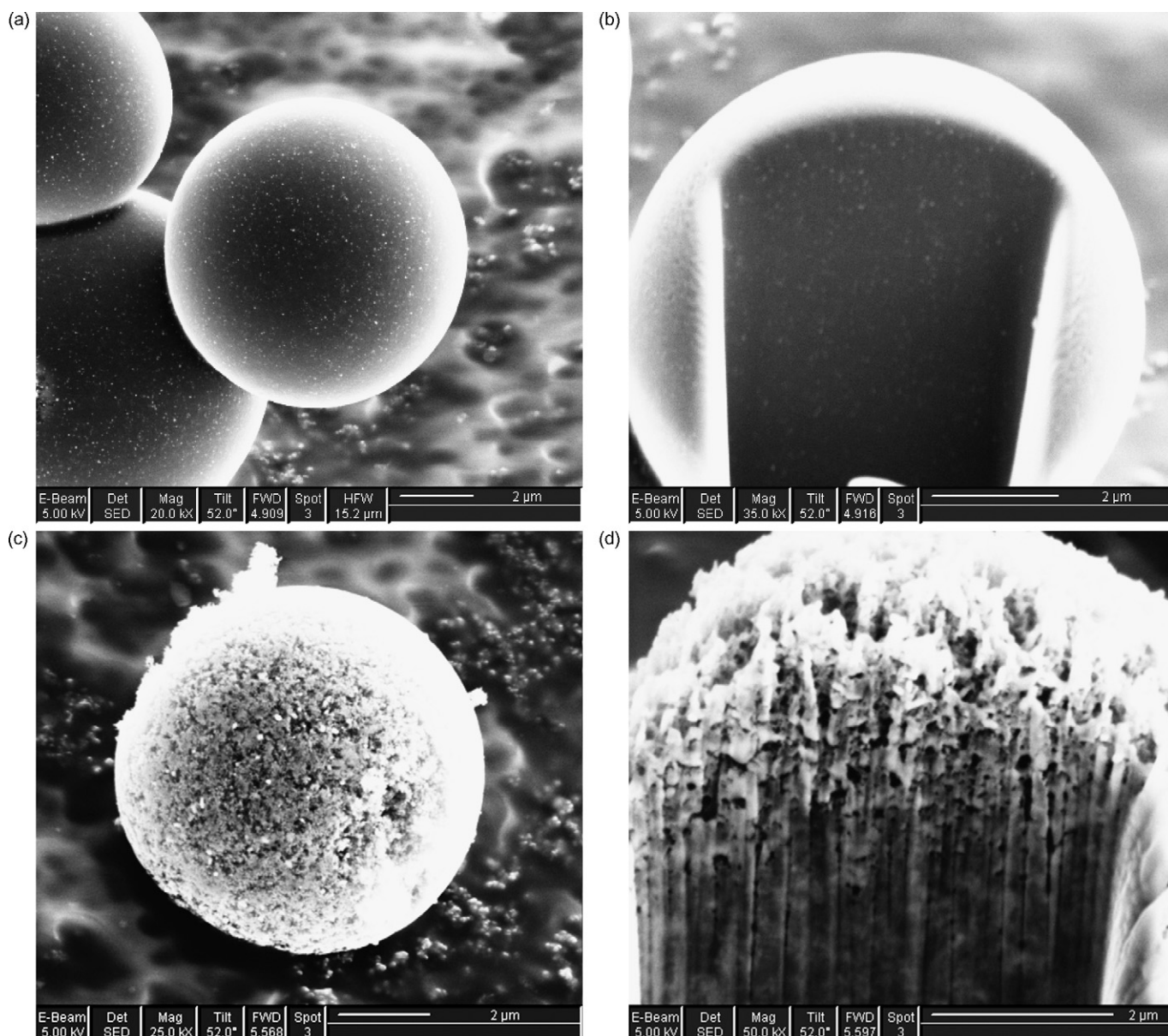

Fig. 1. SEM images of HCS before (a and b) and after (c and d) exposing to H$_2$O vapor.

(Fig. 1b). The surface of the HCS particles becomes rough after H_2O vapor activation (Fig. 1c). Meanwhile, mesopores (20–60 nm in diameter) are found interconnected throughout the HCS particle (Fig. 1d). The mesopores were formed mainly around the iron particles via the reaction of carbon and H_2O vapor. Marsh et al. [8] believed that iron acted as an oxygen-transfer medium in the activation process. However, H_2O vapor activation does not change the chemical properties of the iron itself.

Fig. 2 shows the XRD pattern of an HCS–Sn–C electrode sheet. The peaks at *ca*. 43.2, 50.4 and 74.0° belong to the copper support. All the other peaks can be indexed to Sn. No signals for Fe and hard carbon are detected, probably due to their poor crystallinity.

SEM imaging indicates that the Sn nanoparticles are homogeneously distributed on the HCS (HCS–Sn). Only slight aggregation of the Sn nanoparticles is observed (Fig. 3a). Energy dispersion spectroscopy (EDX) shows that the Sn content is about 10 wt.% in the composite. As the mesopores are interconnected with each other, a lot of tin nanoparticles are expected to be found within the HCS particles. The HCS–Sn was coated with a layer of soft-carbon because the naked Sn nanoparitcles
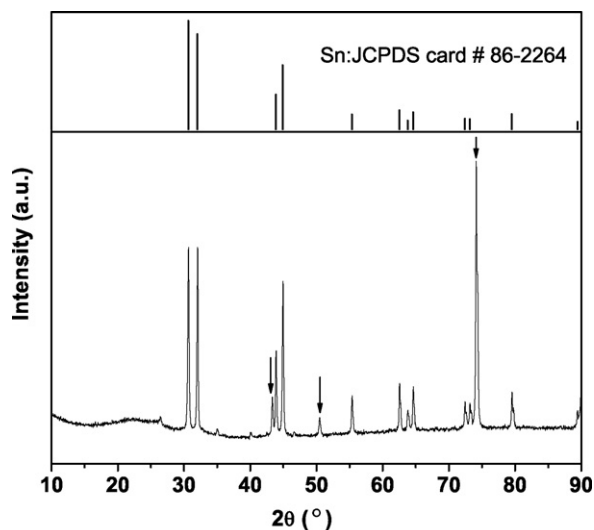

Fig. 2. The XRD pattern of the HCS–Sn–C composite.
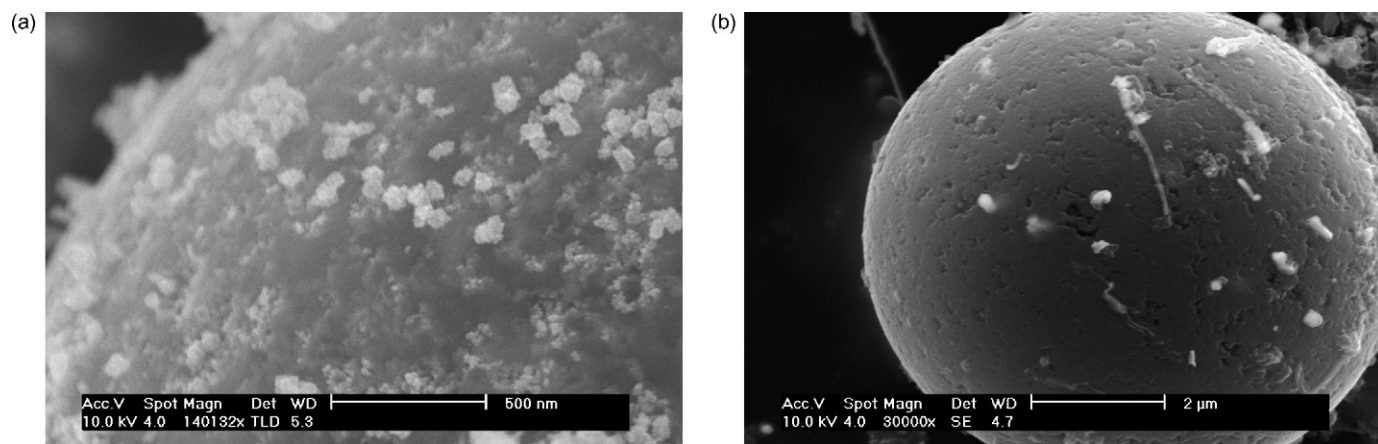

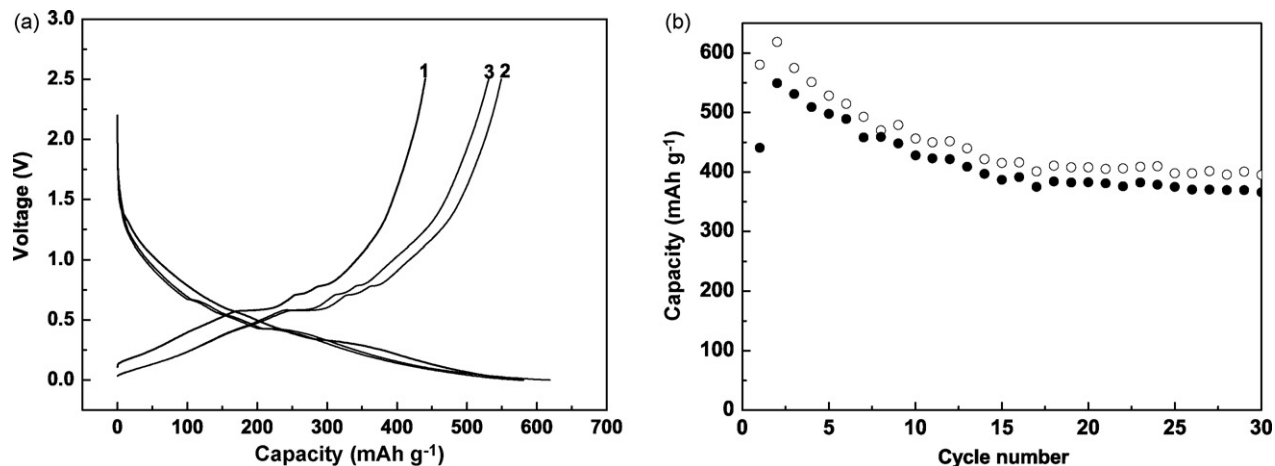Fig. 3. SEM images of HCS–Sn (a) before and (b) after soft-carbon coating.

Fig. 4. The voltage profiles of the HCS–Sn–C electrode in the first three cycles (a) and its cycling performance (b) between 0.0 and 2.5 V (open circle for discharge capacity while the solid dot for charge capacity).
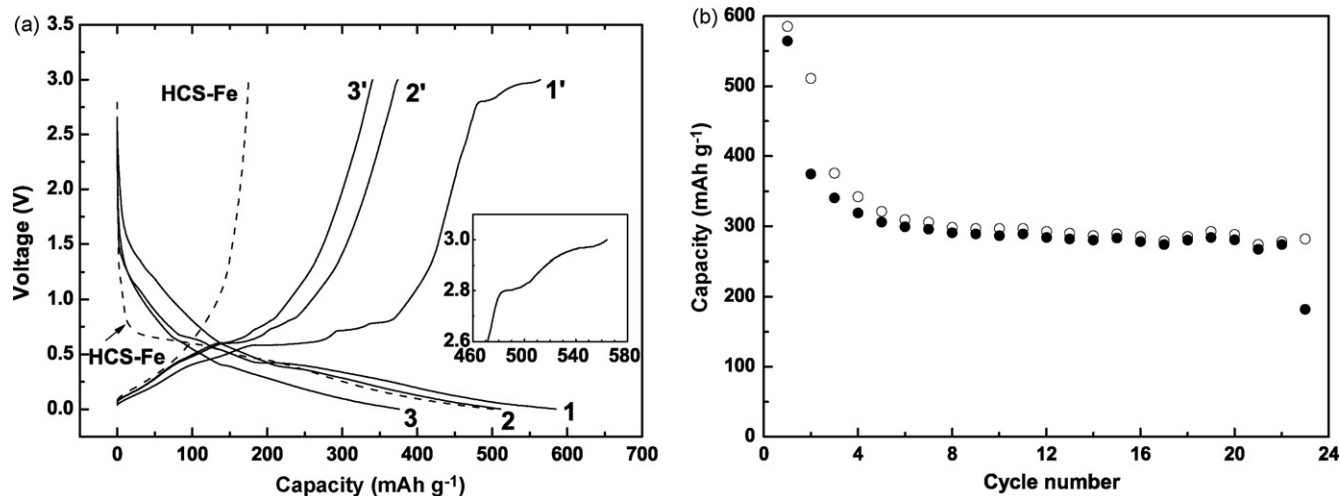
Fig. 5. (a) The galvanostatic voltage profiles of the as-prepared Fe-containing HCS (HCS–Fe) in the first cycle (dashed line) and HCS–Sn–C in the first three cycles (the inset is cut from the charge plateau of HCS–Sn–C in the high-potential range of the first cycle) and (b) the cycling performance of HCS–Sn–C (open circle for the discharge capacity while solid dot for the charge capacity).

tend to be oxidized in air. Fig. 3b shows the SEM image of the soft-carbon-coated HCS–Sn (HCS–Sn–C) particle. It is seen that the HCS–Sn particle is efficiently coated with the soft-carbon. Of course, soft-carbon coating improves the electric conduction of the composite as well.

The electrochemical properties of the HCS–Sn–C composite as anode material for lithium ion batteries are evaluated by galvanostatic charge–discharge cycling. Fig. 4 shows the cycling performance of the HCS–Sn–C between 0.0 and 2.5 V (vs. Li). The complex charge/discharge voltage plateaus below 1.5 V are attributed to the complicated lithiation/delithiation of the hard carbon and tin (Fig. 4a) [10,11]. The initial discharge and charge capacities are 580 and 440 mAh g^{-1}, respectively, corresponding to a coulombic efficiency of 76%. In the subsequent cycles, the coulombic efficiency increases to above 90%. The capacity of the HCS–Sn–C composite fades to 400 mAh g^{-1} after 30 cycles (Fig. 4b). Compared with the cycling performance of pure Sn [12], embedding nano-Sn particles in porous HCS is an effective way to improve the cycling performance of the composite material. This improvement is attributed to two factors. On one hand, the mesopores of the HCS provide sufficient room for the nano-Sn particles to expand during Li insertion because these pores are only partially filled with nano-Sn particles. On the other hand, embedding nano-Sn particles in the mesopores of the HCS hinders the aggregation of the Sn nanoparticles during cycling.

Fig. 5a shows the voltage profiles of the HCS–Sn–C composite between 0.0 and 3.0 V (vs. Li). Different from the voltage profiles of other anode materials, two charge plateaus are observed above 2.8 V in the first charge. The total charge capacity corresponding to these two plateaus is ca. 90 mAh g^{-1}. Therefore, the presence of these two abnormal plateaus makes the initial coulombic efficiency of the composite increase to 96%. This is a value much higher than that of any other reported anode materials, usually between 60% (for the hard carbons and metal oxides) and 85% (for the graphites). These two plateaus

disappear in the subsequent cycles. No such charge plateaus were observed when the active material were replaced with hard carbon/micro-Sn composite or the as-prepared Fe-containing HCS material (Fig. 5a). Hard carbon/micro-Sn composite was also prepared by adding SnCl$_4$ into the sugar solution for the hydrothermal reaction. Microscaled rather than nanoscaled Sn particles were obtained on the surface of HCS because the melting point of Sn is low. This means that those charge plateaus are related to the Sn nanoparticles in the HCS–Sn–C composite electrode rather than due to the oxidation of the Cu foil at high potentials or the catalysis effect of the residual iron in the HCS. However, the cycling performance of the cell charged to 3.0 V is not as good as the one charged to 2.5 V (Fig. 5b). Its coulombic efficiency in the second cycle becomes 73%. From the third cycle on, however, the efficiency increases to more than 91%. The capacity fades to ca.300 mAh g^{-1} after 23 cycles.
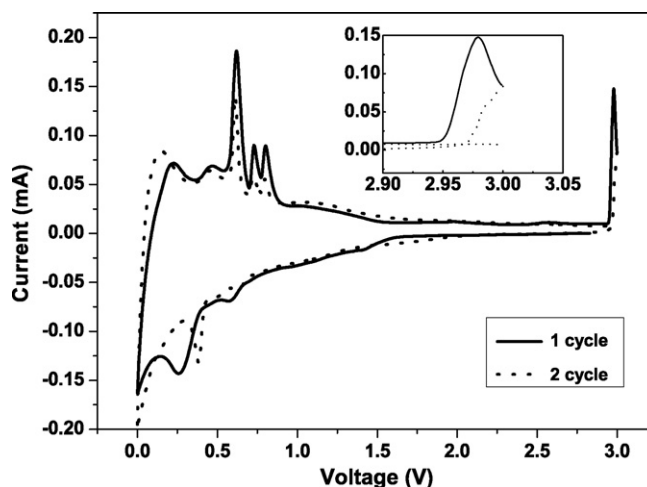

Fig. 6. CV profiles of an HCS–Sn–C electrode (the inset is for the high-potential oxidation peak in the first cycle).
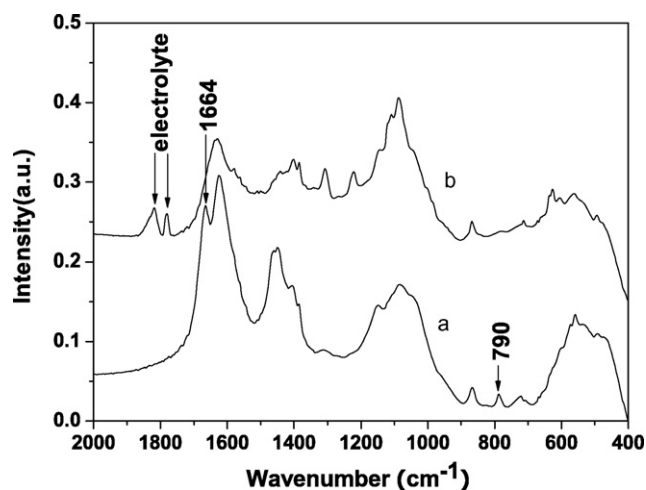
Fig. 7. FTIR spectra of HCS–Sn–C electrode discharged to 0.0 V and then charged to 2.7 V (a) and 3.0 V (b).

The presence of the oxidation plateau above 2.8 V in the first charge process is verified by cyclic voltammetry of another HCS–Sn–C/Li test cell (Fig. 6). In the first charge, a very strong oxidation peak appears at about 2.97 V. However, no corresponding reduction peak is observed in the subsequent discharge process. Nor does the oxidation peak reappear in the subsequent charge processes.

Fig. 7 compares the FTIR spectra of two HCS–Sn–C electrodes first discharged to 0.0 V and then charged to 2.7 and 3.0 V, respectively. Comparing the FTIR spectra of the electrodes charged to different potentials, it is seen that the absorbance peaks characteristic of $ROCO_2Li$ [2,3,13,14] at 790 and 1664 cm^{-1} disappear when the cell is charged to 3.0 V. This means that the $ROCO_2Li$ species in the SEI layer formed during the first discharge are decomposed when the cell is charged to 3.0 V. To our knowledge, there has been no report that the SEI layer can be obviously decomposed below 3 V.

Balaya et al. [15] reported that the SEI film on the reduced Ru particles can be significantly decomposed at and above 3.8 V according to their TEM observations. Due to this decomposition, the initial coulombic efficiency of RuO_2 anode material reached 99%. However, they failed to report the coulombic efficiency in the following cycles. The specific capacity of their RuO_2-based composite anode faded very rapidly. Considering that Ru has a stronger catalytic power than Sn does and that the decomposition voltage of the SEI film is much lower in the present work than in theirs, the decomposition of the SEI film is really surprising and very interesting.

The decomposition of the SEI layer is attributed to the inductive effect of the Sn nanoparticles with high activity. This effect disappears in the subsequent cycles probably because some of the Sn nanoparticles on the HCS surface are interconnected in the second recharge process. This suggestion is supported with the fact that the initial coulombic efficiency of HCS/micro-Sn composite anode is only 62%, consistent with the initial coulombic efficiency of most hard carbon and metal oxide anode materials. Nevertheless, the variation of morphology and structure of Sn cannot be analyzed at present because the Sn nanoparticles

are embedded in the mesopores of a much bigger HCS particle and the HCS particle is coated with a layer of soft-carbon. Anyway, the above observations indicate that it is possible to increase the initial coulombic efficiency of the lithium ion batteries by fixing some Sn nanoparticles on and in the electrode material. Of course, the decomposition potential of the SEI layer is currently still too high to be practical for a real lithium ion battery. However, we find a method that can remarkably increase the initial coulombic efficiency of the anode materials. The Sn-induced decomposition of the SEI film is superior to that by Ru because (1) Sn is much cheaper than Ru or Ru oxides; (2) the decomposition voltage of the SEI on nano-Sn is lower than on nano-Ru; (3) the reversibility of the Sn-HCS composite is much better than that of the RuO_2-based composite anode; Balaya et al. [15] reported that their RuO_2-based composite electrode can only cycle three times; (4) Sn is electrochemically active but Ru is not. There might exist other materials that can induce/catalyze the SEI decomposition at lower potentials. In this way, both the initial coulombic efficiency and the volumetric specific capacity of the lithium ion batteries can be dramatically increased.

4. Conclusions

Tin nanoparticles were embedded in the mesopores of hard carbon spherules activated with H_2O vapor. Such composite material shows high-lithium storage capacity and good cycling performance when cycled between 0.0 and 2.5 V. The tin nanoparticles induce the decomposition of the $ROCO_2Li$ species in the SEI layer when the material is charged to 3.0 V. The tin-induced decomposition of the SEI layer increases the initial coulombic efficiency of the anode material to 96%. This may be a promising way to increase the coulombic efficiency of the anode material and the capacity density of lithium ion batteries though there are still quite some questions remaining unclear.

References

[1] I. Grigoriants, A. Soffer, G. Salitra, D. Aurbach, J. Power Sources 146 (2005) 185.
[2] D. Aurbach, B. Markovsky, A. Shechter, Y. Ein-Eli, J. Electrochem. Soc. 143 (1996) 3809.
[3] D. Aurbach, Y. Ein-Eli, B. Markovsky, A. Zaban, J. Electrochem. Soc. 142 (1995) 2882.
[4] M. Egashira, H. Takatsuji, S. Okada, J.-I. Yamaki, J. Power Sources 107 (2002) 56.
[5] H. Li, Q. Wang, L.Q. Chen, X.J. Huang, Chem. Mater. 14 (2002) 103.
[6] X.D. Wu, Z.X. Wang, L.Q. Chen, X.J. Huang, Carbon 42 (2004) 1965.
[7] R.Z. Yang, Z.X. Wang, J.Y. Liu, L.Q. Chen, Electrochem. Solid State Lett. 7 (2004) A496.

[8] H. Marsh, M.A. Diez, K. Kuo. In: J. Lahaye, P. Ehrburgor (Eds.), Kluwer, Academic Publishers, 1991, p. 205.

[9] Q. Wang, H. Li, L.Q. Chen, X.J. Huang, Carbon 39 (2001) 2211.

[10] Q. Wang, H. Li, L.Q. Chen, X.J. Huang, Solid State Ionics 43 (2002) 152.

[11] R.A. Huggins, J. Power Sources 81–82 (1999) 13.

[12] W. Choi, J.Y. Lee, B.H. Jung, H.S. Lim, J. Power Sources 136 (2004) 154.

[13] D. Aurbach, B. Markovsky, I. Weissman, E. Levi, Y. Ein-Eli, Electrochim. Acta 45 (1999) 67.

[14] Z.X. Wang, X.J. Huang, L.Q. Chen, J. Electrochem. Soc. 151 (2004) A1641.

[15] P. Balaya, H. Li, L. Kienle, J. Mairer, Adv. Funct. Mater. 13 (2003) 621.